Title
The Optimization of Intestinal Epithelial Stem Cell Growth using a Parabolic Response Surface (PRS)

Author
Hantuli, Mohammed Mazen

Publication Date
2016

UNIVERSITY OF CALIFORNIA

Los Angeles

The Optimization of Intestinal Epithelial Stem Cell Growth using a Parabolic Response Surface (PRS)

A thesis submitted in partial satisfaction

of the requirements for the degree

Master of Science in Bioengineering

by

Mohammed Mazen Hantuli

2016

ABSTRACT OF THE THESIS

The Optimization of Intestinal Epithelial Stem Cell

Growth using a Parabolic Response Surface (PRS)

by

Mohammed Mazen Hantuli

Master of Science in Bioengineering

University of California, Los Angeles, 2016

Professor James C.Y. Dunn, Chair

Culturing human intestinal stem cells from individual patient samples holds much promise within the realm of research or therapeutic applications. However, performing in-vitro experiments require a great deal of time, money, and effort. Often times researchers seek to reduce such factors by optimizing certain variables in the simplest and most efficient ways possible. In this experiment, growth conditions are optimized for human intestinal stem cells—derived from patient samples—grown in a 3-D matrigel environment. The method used for the optimization of growth factors, utilizes a Parabolic Response Surface (PRS) assisted by an Orthogonal Array Composite Design (OACD) to derive a second order equation that models spheroid growth, and aids in the discovery of the most efficient culture conditions. It was discovered that R-Spondin, the single most expensive component in culture, was able to be

reduced by 50% and still produce spheroid numbers similar to standard/conventional conditions. This in turn translated to a 40-50% reduction in cost. It was also discovered that cell passaging and sample variation can heavily influence optimization results.

The thesis of Mohammed Mazen Hantuli is approved.

Benjamin M. Wu

Dean Ho

James C.Y. Dunn, Committee Chair

University of California, Los Angeles

2016

Table of Contents

LIST OF FIGURES

ACKNOWLEDGEMENTS

I would like to give thanks and praise to God for giving me the opportunity, resources, and will to embark upon this journey at UCLA. I of course, would like to thank my family, mainly Mom and Dad, for their unwavering love and support.

I would also like to express gratefulness and appreciation to my advisor Dr. James Dunn for his guidance throughout this project. His knowledge and patience allowed for me to grow as both a researcher, and as an individual. I would also like to thank my fellow lab members at Dr. Dunn's lab, whose continuous support and knowledge helped me move forward. I would especially like to thank Tommy Nguyen for his help in data collection and analysis. This project would not have been possible if it weren't for the support and collaboration of Dr. Chih-Ming Ho and Dr. Dean Ho and their lab group members, especially Theodore Kee.

INTRODUCTION

The human body is truly unique in the way it is able to grow, repair, & defend itself from various elements that pose a potential risk. Such processes require various chemical reactions, which it turn require energy. This is where the role of the intestinal system comes into play; it is crucial in the breaking down of food and subsequent uptake of nutrients and energy. This however leads to an unforgiving environment where pH fluctuations and other factors can lead to tissue degradation. As a result, the epithelial layer of the small intestine is constantly destroyed and renewed. The renewal of the epithelial layer is made possible by the presence of adult intestinal stem cells [1,2]. These cells reside within the crypts of Lieberkühn, which are situated below the villi. Studies have identified the leucine-rich-repeat-containing G-protein-coupled receptor 5 (Lgr5) as a marker for the intestinal stem cells [3]. In crypts, Lgr5+ cells reside within a specialized microenvironment, also known as a "niche". The niche contains Paneth cells that associate with Lgr5+ cells and give the necessary factors for renewal and growth. These factors include: EGF, TGF-α, Wnt3, and Notch ligand Dll4 [2,5,8]. Another type of stem cell population are referred to as +4 cells. These cells unlike Lgr5+ cells do not actively divide and give rise to other cell types, but rather, they are believed to play a role in reviving Lgr5+ cell population in the event of an injury [2,7].

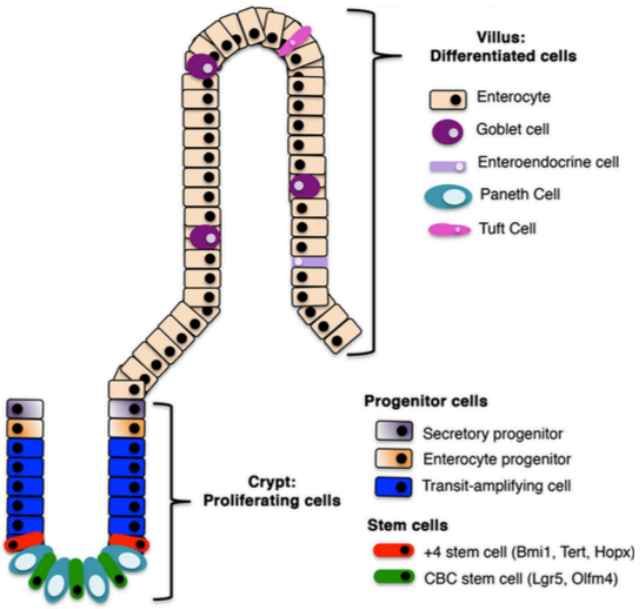

Figure 1. Intestinal cell differentiation & migration

(Image adapted from Elliot &Kaestner, 2015 [7])

Prior interest has been expressed in the culturing of Lgr5+ cells, however, understanding and replicating the niche conditions is critical. The creation of an artificial in-vitro niche environment, is made possible by the addition of exogenous growth factors to intestinal stem cell culture media. However, this application is established for mouse cell culture [4]. The exact concentrations for the growth components of human intestinal cells remains unclear. This calls to attention the need to optimize the combinatorial growth factor concentrations for the application of *in-vitro* human intestinal stem cell-culture.

It is highly difficult, impractical, and costly to experiment with all of the possible combinations of growth components in a given cell culture system. This highlights the need to explore various published methods used to optimize both in-vitro and in-vivo experimental systems. Promising past optimization approaches utilize Feedback System Control (FSC)-based experiments to find the best cocktails needed for various applications. The applications range

from drug delivery nano-diamonds to liver transplant immunosuppressant drug cocktails. In those studies, the FSC platform produced response surfaces that were parabolic [11, 12]. A promising application is an optimization protocol of an anti-retroviral drug cocktail used to treat Herpes Simplex Virus Type-1 (HSV-1) [11-13]. In that protocol, multiple statistical Design of Experiment (DOE) approaches are combined and used with a 2^{nd} order polynomial, in order to optimize drug-cocktail concentrations in just one iteration [11]. Xu et. al (2014) outlines a general guideline for constructing an Orthogonal Array Composite Design (OACD) that can be tailored to fit nearly any multi-factor experiment. The OACD assists in creating a parabolic response surface. This approach will be explored and applied to the optimization of human intestinal cell culture media.

OBJECTIVE

The main objective of this project is to utilize an efficient, reliable, and general platform in order to optimize growth conditions for human intestinal stem cells. This could not only reduce the cost associated with culturing these cells, but also potentially lead to increased growth. Another objective is to observe what other factors can play a role in affecting the results of this experiment.

MATERIALS & METHODS:

Experiment Outline

The initial step to optimizing growth factor concentrations, relies on the ability to screen the various components in question. Prior to the screening stage, however, minimum and maximum/threshold concentrations for each component had to be established. The minimum concentration was defined as the concentration by which no spheroid growth was observed, while the maximum concentration was classified as the most economically feasible maximum concentration at which the change in spheroid growth numbers is minimized (i.e. spheroid numbers plateaued). This task was accomplished by measuring the output, intestinal spheroid growth, as a result of varying one component, while holding all other components constant. For example, in order to determine the maximum concentration for the EGF component, Noggin, R-Spondin, and Y-inhibitor were each held constant at the "standard" or previously set concentration from prior literature (Sato 2009). The experimental max & min. values for each individual component was then plugged into an Orthogonal Array Composite Design (OACD), which consists of a combination of a 2-level fractional factorial design and a 3-level orthogonal array. The 2-level portion of the OACD accommodates for the maximum and minimum concentration values, while the 3-level component accommodates for both the maximum and minimum concentration as well, but it also integrates a mid-level concentration. Cell culture media was then prepared according to the concentrations set forth by the OACD. Cells were grown in duplicate wells for each condition for approximately 7 days. The intestinal spheroids

were then quantified and the response profile was then utilized in order to develop coefficients for a 2nd order polynomial modeling spheroid growth. After the establishment of the 2nd order equation, linear regression was performed and many potential factor combinations were attained. The suggested combinations with the highest predicted spheroid numbers and lowest costs were considered.

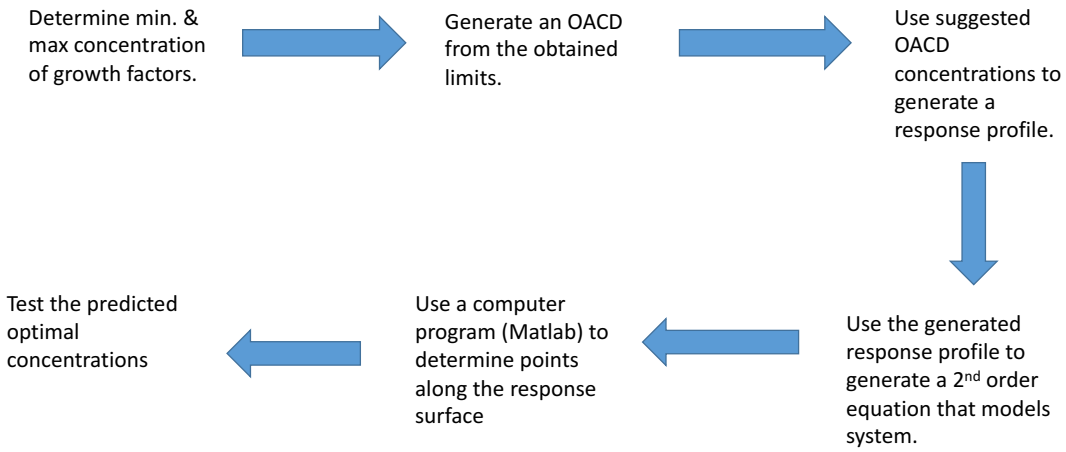

Figure 2. Experiment Outline

OACD

The approach used in this experiment is based on the idea of using an Orthogonal Array Composite Design (OACD) in order to choose the inputs that will give rise to a parabolic response surface. An OACD consists of an orthogonal array (OA) and a fractional factorial design [11-13]. Xu et. al, 2014 [11] demonstrated the efficiency of combining popular optimization methods to form the OACD. The OACD used by Xu et. al [11], comprised of a 16-

run fractional factorial (2-levels) and an 18-run orthogonal array (3-levels). It was constructed based on the number of factors, levels, and resolution desired (Figure 3). The 2-level fractional factorial portion is crucial in analyzing the main effects and the interaction between 2 factors [11,14]. We are capable of estimating higher order interactions, however, interactions between 3 factors or more are considered negligible, so for practicality's sake, they are ignored [14]. An orthogonal array (OA) can be used to determine the quadratic effects. If one were to use the Taguchi design method, which utilizes OA, as opposed to an OACD, the interaction terms would be neglected. The Taguchi design method would also incorporate a search area that cannot be fitted to the equation used at a later stage [11,14]. The minimum and maximum values obtained from the prior factor screening stage, were then plugged into the OACD.

	2-level factorial portion			3-level OA	
k	Design	n_c	Columns and generators	Design(n_a)	Columns
3	2^3	8	-	OA(9)	(1-3)
3	2^{3-1}_{III}	4	$C = AB$	OA(9)	(1-3)
4	2^4	16	-	OA(9)	(1-4)
4	PB(12)	12	(1-4)	OA(9)	(1,3,4,2)
4	2^{4-1}_{IV}	8	$D = ABC$	OA(9)	(1-4)
5	2^{5-1}_{V}	16	$E = ABCD$	OA(18)	(2-6)
5	PB(12)	12	(1-5)	OA(18)	(2,5,3,4,6)
5	2^{5-2}_{III}	8	$D = ABC, E = AB$	OA(18)	(2-4,6,5)
6	2^{6-1}_{VI}	32	$F = ABCDE$	OA(18)	(1-6)
6	PB(20)	20	(1-5,13)	OA(18)	(1,4,6,3,2,5)
6	PB(12)	12	(1-5,7)	OA(18)	(2,5,3,4,6,1)
7	2^{7-1}_{VII}	64	$G = ABCDEF$	OA(18)	(1-7)
7	2^{7-2}_{IV}	32	$F = ABCD, G = ABE$	OA(18)	(1,2,5,3,4,7,6)
7	PB(20)	20	(1-5,13,16)	OA(18)	(3,1,5,7,4,2,6)
8	2^{8-2}_{V}	64	$G = ABCDE, H = ABCF$	OA(27)	(1-8)
8	2^{8-3}_{IV}	32	$F = ABCD, G = ABE, H = ACE$	OA(27)	(1,3,4,5,2,7,8,6)
8	PB(20)	20	(1-5,13,16,15)	OA(27)	(6,3,8,4,2,1,7,5)
9	2^{9-2}_{V}	128	$H = ABCDE, J = ABCFG$	OA(27)	(1-9)
9	2^{9-3}_{IV}	64	$G = ABCDE, H = ABCF, J = ADF$	OA(27)	(1,3,8,2,6,7,5,4,9)
9	2^{9-4}_{IV}	32	$F = ABCD, G = ABE, H = ACE, J = ADE$	OA(27)	(5,6,1,7,2,4,9,3,8)
10	2^{10-3}_{V}	128	$H = ABCDE, J = ABCFG, K = ABDF$	OA(27)	(1-10)
10	2^{10-4}_{IV}	64	$G = ABCDE, H = ABCF, J = ADF, K = ABEF$	OA(27)	(5,6,8,2,3,4,10,7,9,1)
10	2^{10-5}_{IV}	32	$F = ABCD, G = ABE, H = ACE, J = ADE, K = BCDE$	OA(36)	(7,6,3,2,9,1,10,8,5,4)

Figure 3. OACD table

A general table outlining the construction of an OACD. (Adapted from Xu et. al, 2014 [11])

2nd Order Model

$$y = \beta_0 + \sum_{i=1}^{k} \beta_i x_i + \sum_{i=1}^{k} \beta_{ii} x_i^2 + \sum_{i=1}^{k-1} \sum_{j=i+1}^{k} \beta_{ij} x_i x_j + \epsilon$$

Equation adapted from Jaynes et. al, 2013 [14]

In this equation, β represent the coefficients for each term. This equation aids in appreciating the need for both a 2-level fractional factorial portion and an OA component. The second-order term is dependent on the OA portion, while the first-order terms (linear and interaction terms) are dependent on the factorial portion [11].

Cell Culture

Growth Media Preparation

(Note: Concentrations listed are the standard "1x" concentrations)

- 50% 2x media:
  - 1xN2
  - 1xB27
  - Hepes (10mM, Invitrogen)
  - 1xABAM (Invitrogen)
  - Glutamax (2mM, Invitrogen)
  - N-Acetylcysteine (1mM, Sigma-Aldrich)
- 50% HB8 (Human Myofibroblast) condition media.
- EGF (50 ng/mL, Peprotech)
- Noggin (100 ng/mL, Peprotech)
- R-Spondin (1 μg/mL, R&D)
- Y-27632 (10 μM, Stemgent)

Experimental Components:

- GSKi CHIR99021 (5 μM)

- Valproic acid (1mM)
- Benzalkonium Chloride
- Insulin-like Growth Factor (IGF-1)
- Insulin
- Dexamethasone

Passaging

After viewing the well under the microscope and verifying spheroid confluency, the 3-D matrigel droplet is detached from the bottom of the well by aggressive scrapping with the pipette tip. The matrigel along with the media is then transferred to a 1.5 mL Eppendorf tube. The Eppendorf tube is then very briefly spun in a mini-centrifuge 3 times (4 seconds per spin). Once all the cells and matrigel settle to the bottom, all old supernatant is removed, and the pellet is resuspended in 500 μL of TrypLE (Invitrogen). It is then placed in a water bath at 37°C for 5 minutes. Afterwards, the media is quenched with 500 μL 10% FBS DMEM. Next the spheroids are lysed by pipetting the media up and down approximately 40-50 times (depending on spheroid size). A 10 μL sample is then placed on a glass slide and observed under a microscope. The number of particles in that sample is estimated, and an approximation for the total number of particles is made. From the total number of particles, the appropriate particle per well amount is transferred to a new tube, and spun down. The old media is then aspirated, and freshly thawed matrigel is added using cold pipette tips. Once the matrigel is mixed in with the particles, the mixture is then plated onto a 48-well plate (Costar) and placed in an incubator for 15 minutes. Finally, the appropriate growth media is added to each well and changed every other day. (Note: Each condition must be passaged separately.)

Intestinal Crypt Isolation

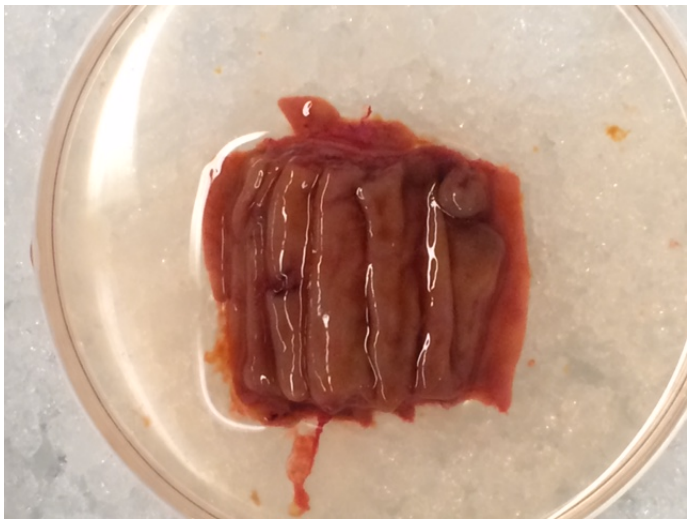

Figure 4. Duodenum sample pre-processing

The isolation of intestinal crypts was performed according to UCLA Intestinal Stem Cell Consortium (ISCC) protocol based on procedure by Sato et al. 2009. Freshly extracted human duodenum samples are placed on a petri dish on ice (Figure 4). It is initially washed with cold PBS to remove debris. Next the muscle layer of the tissue is separated from the mucosal layer using forceps to peel the muscle and a scalpel to cut in between the layers. The muscle layer is then discarded, while the mucosal layer is cut into small pieces (~1x1 cm) using scissors. The pieces are then placed in 30 mL of PBS and vortexed for 30 seconds in 3 second pulses. The supernatant is then aspirated. This washing step is repeated until the supernatant is clear (or mostly clear). Next the pieces are then placed in 30 mL of PBS containing 3mM of EDTA and 1mM of DTT, while carefully rocking at 4°C for 30 minutes. Afterwards, the supernatant is again aspirated and approximately 30 ml of PBS is added and vortexed for 30 seconds in 3 second pulses. The supernatant is then collected in a 15 mL conical vial, and the washing/vortex step is repeated 5 more times for a total of 6 vials. All vials are then centrifuged at 140 rcf at 4°C for a total of 2 minutes, and the supernatant is then removed. A 10% FBS solution is then added

to the pellets that form. The resulting media is then filtered through both a 100 μm and 70 μm cell strainer. The filtered fractions are once again spun at 140 rcf at 4°C and the supernatant is removed and the pellet is re-suspended with basic media (Advanced DMEM/F12, 2mM Glutamax, 10mM Hepes, and 1x ABAM). The resulting crypts are then stored on ice to be used in the seeding process.

Crypt Seeding

A frozen aliquot of matrigel (BD Bioscience) is removed from the freezer and allowed to thaw at 4°C. Meanwhile, a 10 μL sample of the crypts is placed on a glass slide and the crypt/μL concentration is determined after counting under the microscope. An appropriate amount of crypt solution is aliquoted into an Eppendorf tube and centrifuged 3 times for 5 seconds each time. The supernatant is then aspirated and the pellet containing the crypts is re-suspended in matrigel (Note: matrigel can only be handled with frozen pipette tips). 25 μL of matrigel containing 100 crypts are deposited in each well. Each condition contains duplicate wells- one well for passaging and one well for RNA extraction. Once the plating is complete, the culture plate is incubated at 37°C for 15 minutes. The final step consists of adding the appropriate media into each well.

Imaging

Once the cells reach the desired confluency, the 48-well plate is imaged using an Olympus IX73 microscope. A total of 12-15 images (depending on matrigel droplet) of each well is taken from all areas. The resulting images are stitched together to form one large image. It is important that this step is done before the passaging and RNA extraction take place.

RNA Extraction

The RNA extraction approach used is based on an adaptation from a protocol used by Dr. Martin Martin's Research laboratory at UCLA, that utilizes trizol (Invitrogen) and chloroform. The RNA is then quantified using a Nanodrop 2000c. Qiagen RNeasy kit could not be used due to reduced RNA extraction efficiency experienced when extracting small amounts of RNA.

Results & Discussion

Initially, a range of concentrations were explored in an effort to identify the maximum and minimum concentrations in the conversion of intestinal crypts to spheroids. The minimum concentration was defined as the condition at which little to no growth was observed. The maximum condition was determined to be the condition in which the most spheroids formed at an economically feasible concentration. The standard concentration was referred to as 1x, and every deviation from that standard was re-labeled appropriately. For example, half the standard concentration of EGF (50 ng/ml), was re-labeled as 0.5x (25 ng/ml).

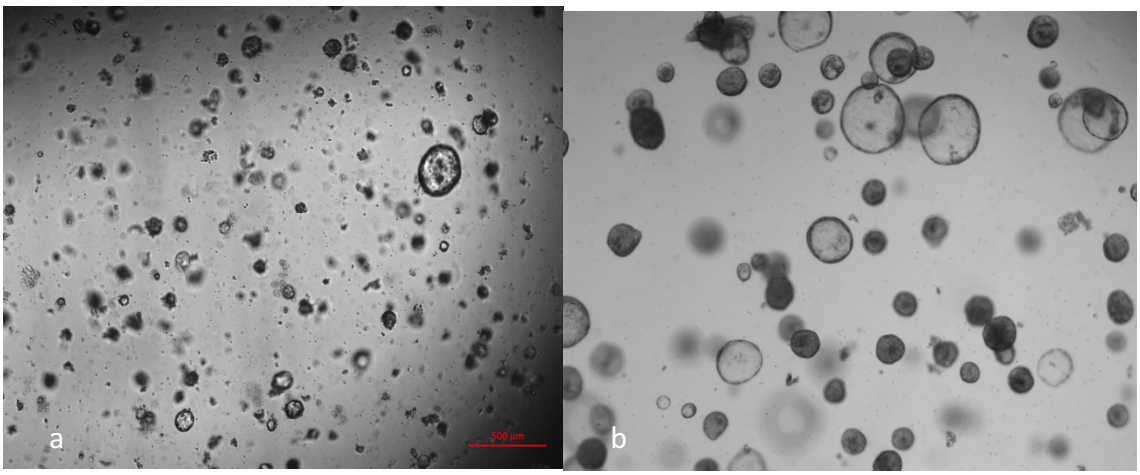

Figure 5. Crypt to Spheroid conversion

a) A sample in which few spheroids formed p0d8. b) A separate sample where spheroids formed p0d6

Factors were screened using crypts (100 crypts/well) from various samples. The initial factor screening was beneficial in predicting the suitability of the optimization model. The

spheroid conversion efficiency varied between samples, making the task of performing a dose response curve difficult. Figure 5 highlights the fact that crypts from two different samples, under the same culture conditions can exhibit quite different behavior. Upon comparison, crypts from figure 5b formed spheroids by passage 0 day 6 (P0D6), while figure 5a showed very scarce spheroid formation by P0D8. Therefore, it was decided that the optimization protocol would best be performed on only one cell line (thawed at P8) that had been established prior to experimentation. The first step was finding the optimal particle to well ratio, obtained from dissociated spheroids during passaging.

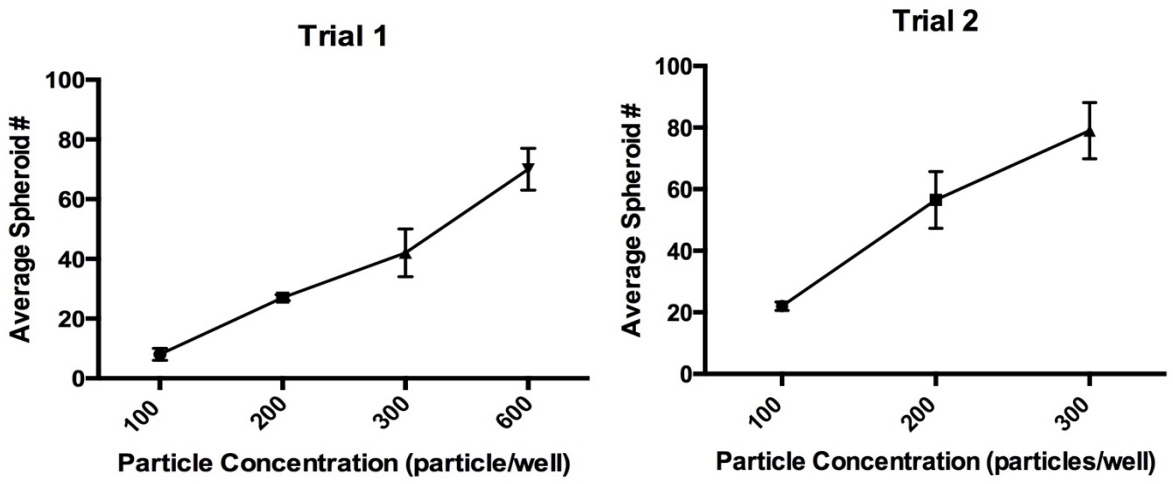

Figure 6. Summary of particle concentration trials

Different particle/well concentration were cultured in the standard (1x) condition and observed for 7 days post passaging. An over-abundance/confluency issue was encountered when the particle concentration was too large. This could influence the output variable (spheroid sount) due to the limited area available for spheroid growth in the 25 µl matrigel droplet. When the particle to well ratio was too low, a low amount of spheroids formed, which affected the ability to observe differences between different growth conditions. After numerous trials, 300

particles/well was determined to be the standard initial concentrations to be used across all conditions for all future experiments. As shown in Figure 6, differences in spheroid numbers were observed between trials, proving that another source of variation was present in the system. Spheroid size differences were also present. However, the optimization model does not account for size as a variable.

The next stage was to determine the maximum and minimum concentrations for EGF, Noggin, R-Spondin, and Y-27632. Dose-response curves were obtained for each factor by varying one component, while holding all others constant.

EGF

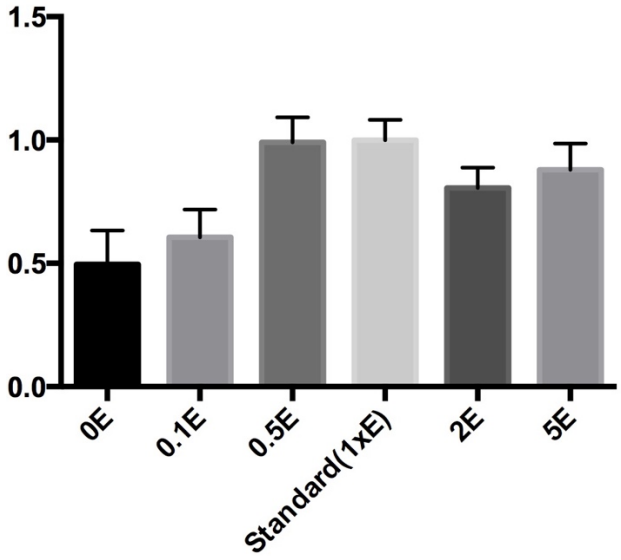

Figure 7. Cumulative EGF data P0-P2 (Normalized to 1x of each trial).

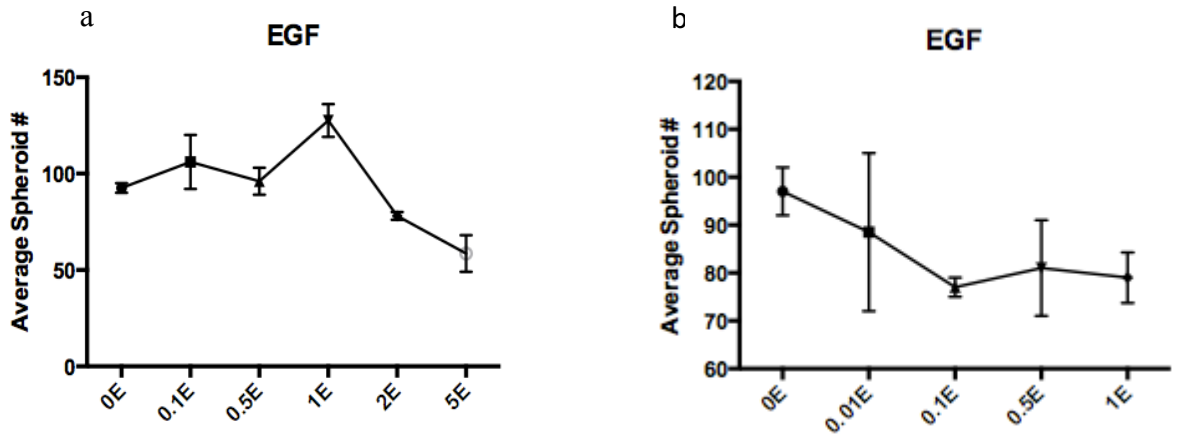

Figure 8. a) P0 Trial 1 b) P0 Trial 2

There seemed to be a difference in both numbers and growth trends between trial 1 and trial 2, while varying the concentrations of EGF at P0. In Figure 8a, trial 1 seems to show a trend until 1xE, but in trial 2, no correlation between concentration and growth is present. Differences in spheroid growth between the conditions was not as apparent until P1 and P2, highlighting the important role that passaging plays. In Figure 7, where cumulative P0-P2 data is shown, an upward trend is displayed after passaging. (Note: Figure 7 Y-axis is unitless due to being normalized). From the displayed data, it was decided that the minimum input value used for the OACD would be 0x and the maximum input value used would be the standard (1x).

Noggin

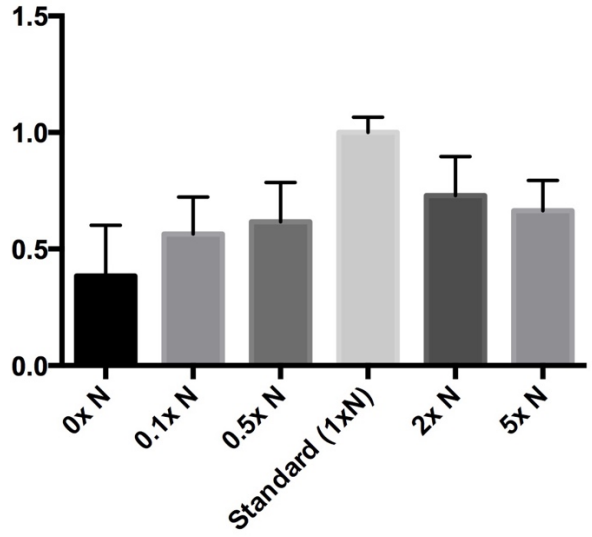

Figure 9. Cumulative Noggin Trials P0-P2 (Normalized to 1x of each trial):

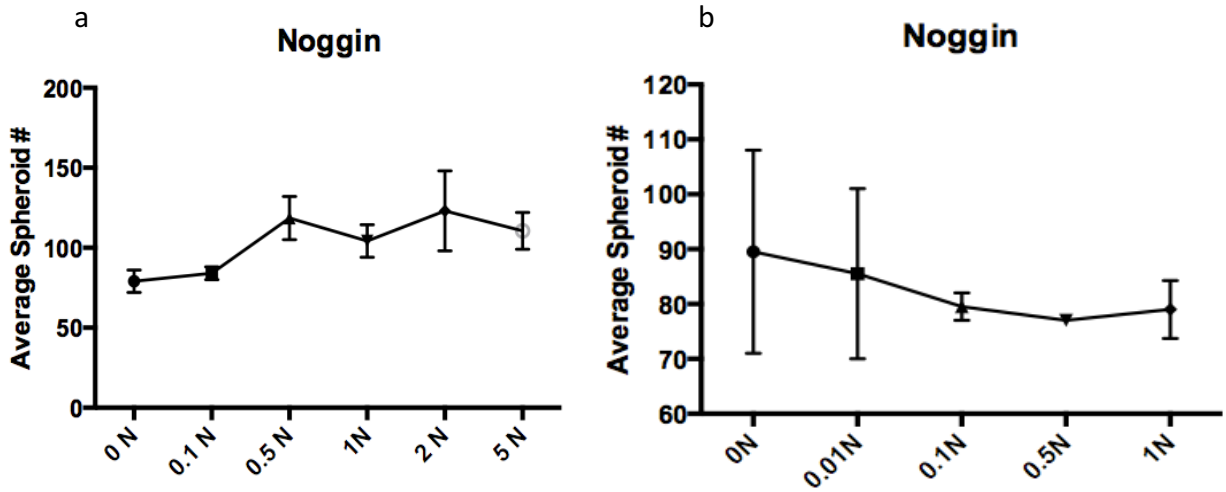

Figure 10. a) P0 Trial 1 b) P0 Trial 2

Establishing a dose-response curve for Noggin proved to be unreliable at P0. However, it was not until the individual conditions were passaged (P1 & P2) did a clear relationship between growth factor concentration and spheroid growth become visible in Figure 9. In Figure 9, the cumulative post-passaging results of each concentration is shown. These results were consistent with the idea that Noggin is necessary for post-passage survival (Sato et al. 2009). Based on the

cumulative data, the minimum concentration was set at 0x and the maximum concentration was set at 1x.

R-Spondin

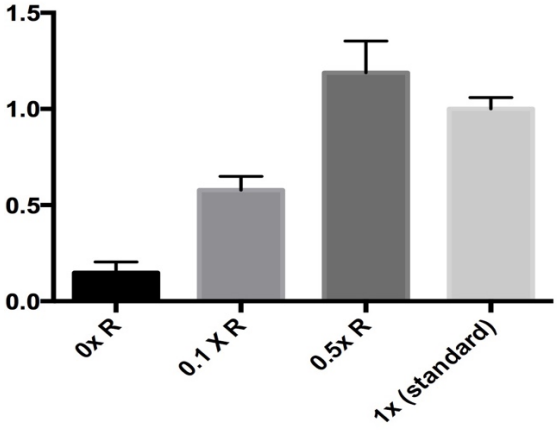

Figure 11. Cumulative R-Spondin Trials P0-P2 (Normalized to 1x of each trial):

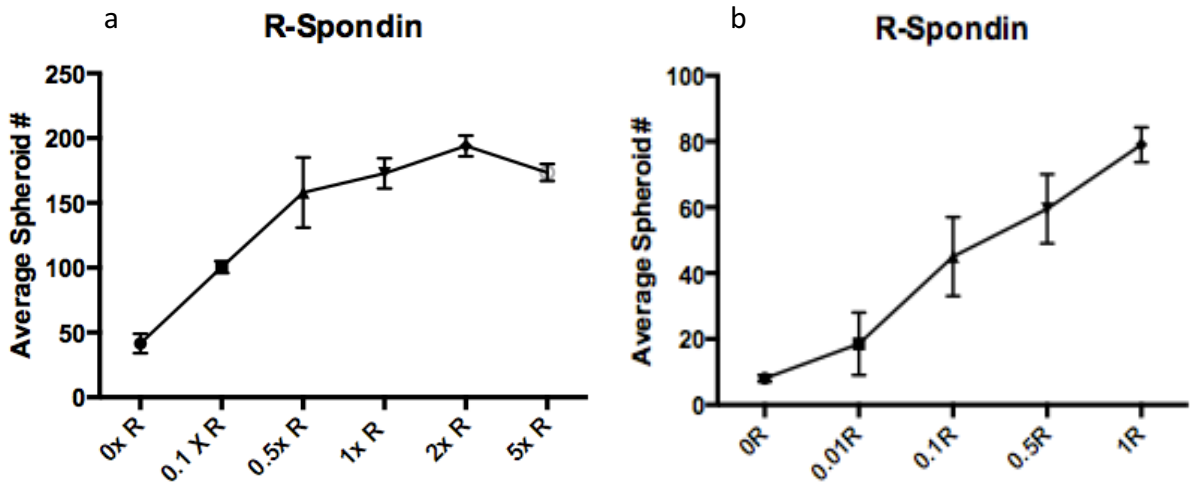

Figure 12. a) P0 Trial 1 b) P0 Trial 2

Spheroid numbers seemed to be directly correlated to the amount of R-Spondin present in culture. With the exception to average number of spheroids, P0 results seemed to be quite similar across both trials. Given that 2xR and 5xR showed growth similar to 1x, at double and 5 times the cost respectively, they were not included in trial 2. After examining P0 data from both trials,

0x was designated as the minimum and 1x as the maximum. Although the normalized cumulative P0-P2 data showed highest growth at 0.5xR, P0 data showed otherwise, and since P0 data was reproducible, it was used to establish the max. and min. values. Nevertheless, the cumulative data significant since it displays that less R-Spondin is possibly feasible for long term culture conditions.

Y-27632

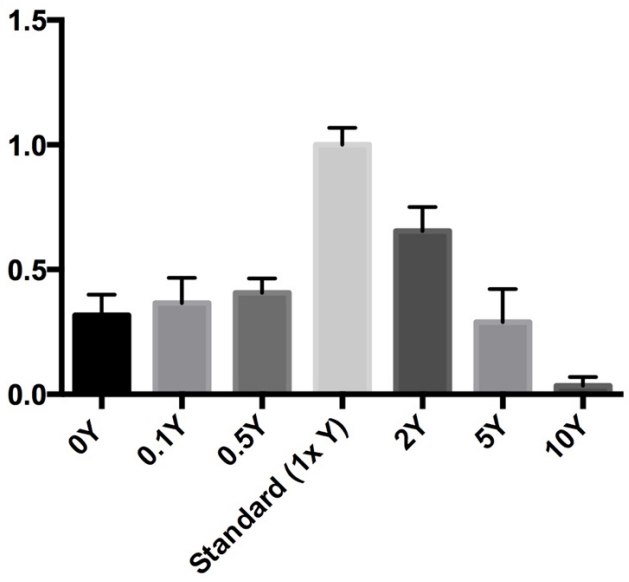

Figure 13. Cumulative Y-27632 trials P0-P2 (Normalized to 1x of each trial):

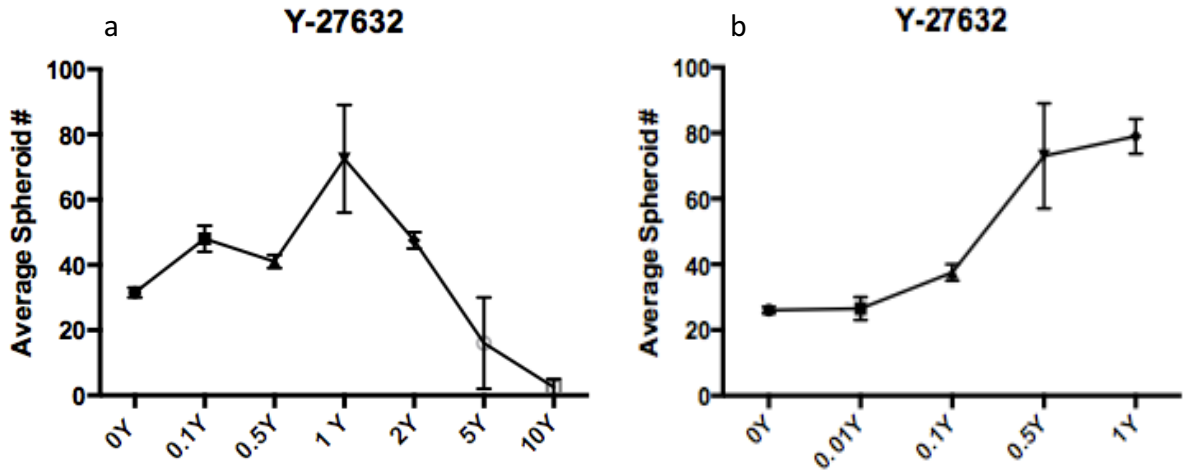

Figure 14. a) Y-27632 P0 trial 1 b) Y-27632 P0 trial 2

Spheroids exposed to a range of Y-27632 concentrations grew the best at 1xY. This result was consistent with both trials at P0 and the cumulative P0-P2 data. The minimum input value for Y-27632 was set at 0x and the maximum input was set at 1x.

Experimental Factors

Other factors that had been tested for their spheroidal growth potential CHIR99021, Valproic Acid (VPA), Insulin Like Growth Factor-1 (IGF-1), Insulin, Dexamethasone, and Benzalkonium Chloride (BAC).

VPA

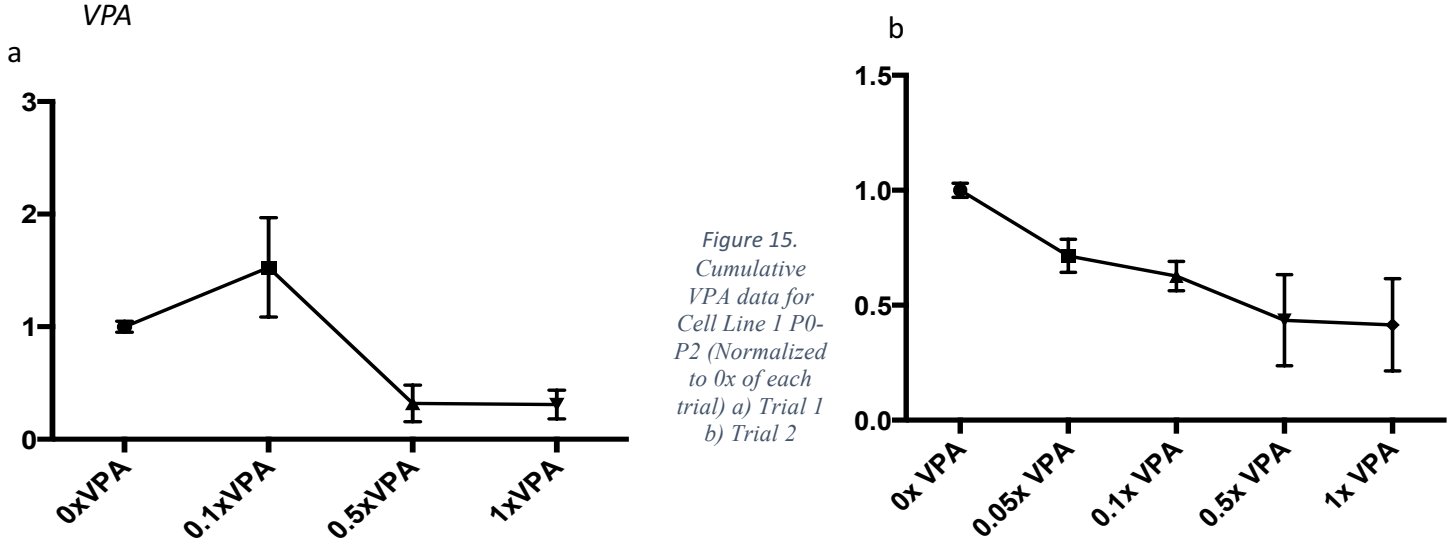

Figure 15. Cumulative VPA data for Cell Line 1 P0-P2 (Normalized to 0x of each trial) a) Trial 1 b) Trial 2

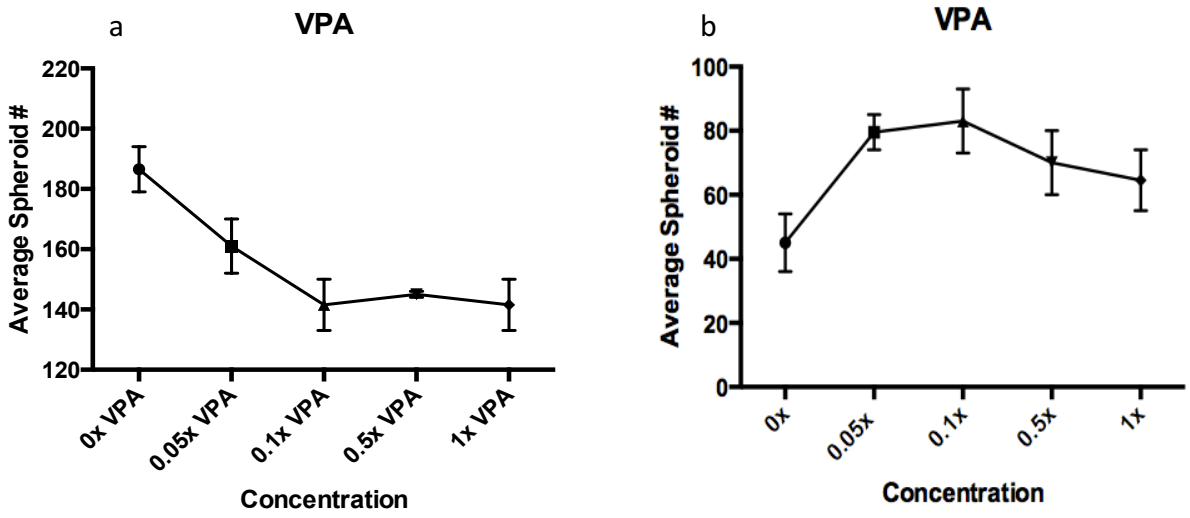

Figure 16. a) P0 Trial Cell Line 1 1 b) P0 Cell Line 2

VPA was tested due to past work from Yin et. al, showing that VPA and CHIR99021 combinedincrease LGR5+ stem cell population [9].With a CHIR99021 concentration held constant at 5 μM, the VPA concentration was varied. In trial 1, the cumlative data for Cell Line 1 showed that 0.1xVPA increased spheroid growth post P2 only, while all other concentrations greatly inhibited growth regardless of passage number. P0 and P1 values of 0.1x did not exhibit growth however. A 0.05x concentration was added upon culturing the cells for a second time. This concentration was added in order to verify that the optimal point was indeed at 0.1x and not at any lower concentrations. Surprisingly, results in trial 2 showed an inhibitory response post-passaging at all levels. When VPA was tested at p0 for Cell Line 2, all levels of VPA seemed seemed to greatly increase growth at P0. VPA supported growth in Cell Line 2, yet inhibited it in another, suggesting that sample variability may be responsible for the results seen.

CHIR99021

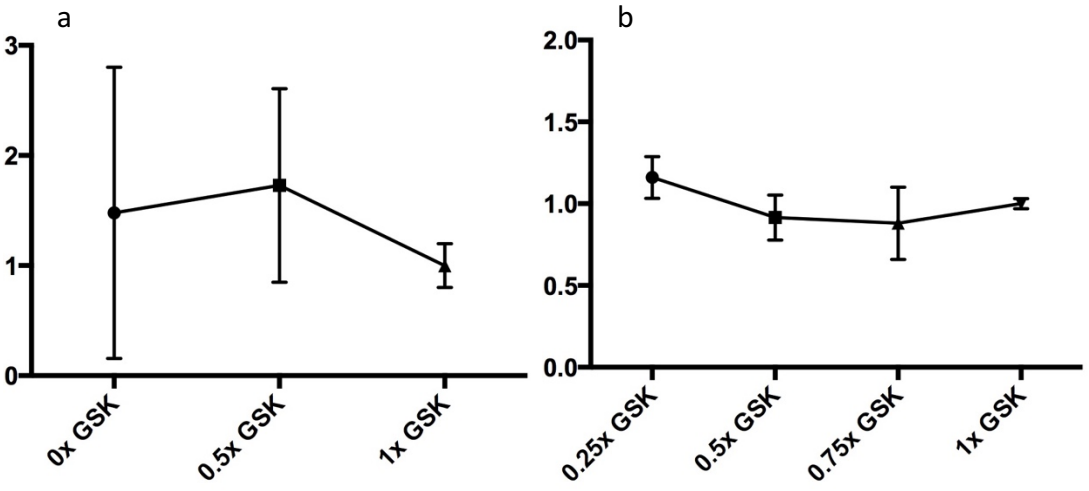

Figure 17. Cumulative CHIR99021 Trials, P0-P2 (Normalized to 1x of each trial). a) Trial 1 b) Trial 2

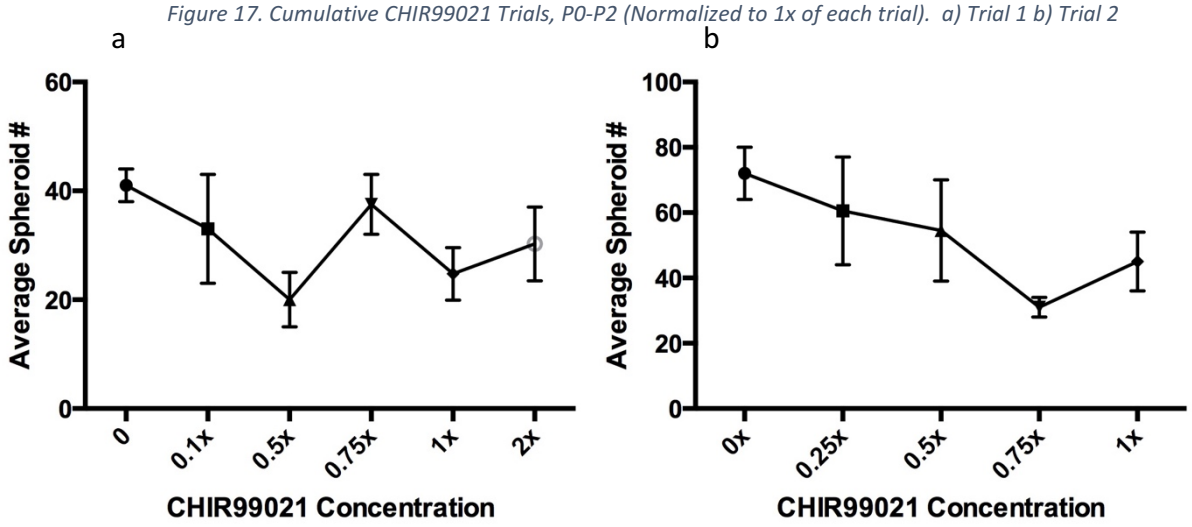

Figure 18. CHIR99021 P0 Trials. a) Cell Line 1 b) Cell Line 2

Past work has shown that the GSK-3β inhibitor activates the Wnt-β-catenin pathway, which increases the number and size of LGR5+ cells [9]. CHIR99021 was added during the first 2 days post-passaging. 1x (5 μM) was used as the standard, since CHIR99021 had been used in prior cultures at this particular concentration. The results did not display any noticeable difference in numbers when concentrations were varied. To further verify that this was the case, and the observed outcome was not restricted to one cell line, another cell line was tested. However, the other cell line (Cell Line 2) displayed a similar outcome. This was surprising, since past

experiences in our lab showed an increase in crypt to spheroid formation when CHIR99021 was added post-plating. Evidence of CHIR99021 support growth on higher passage cell lines is not supported however. Therefore, the use of CHIR99021 was discontinued in the later stages of experimental trials. It is noteworthy that Yin et. al (2014) used CHIR99021 continuously-not just the first 2 days- and only used Y-27632 the first 2 days.

IGF-1

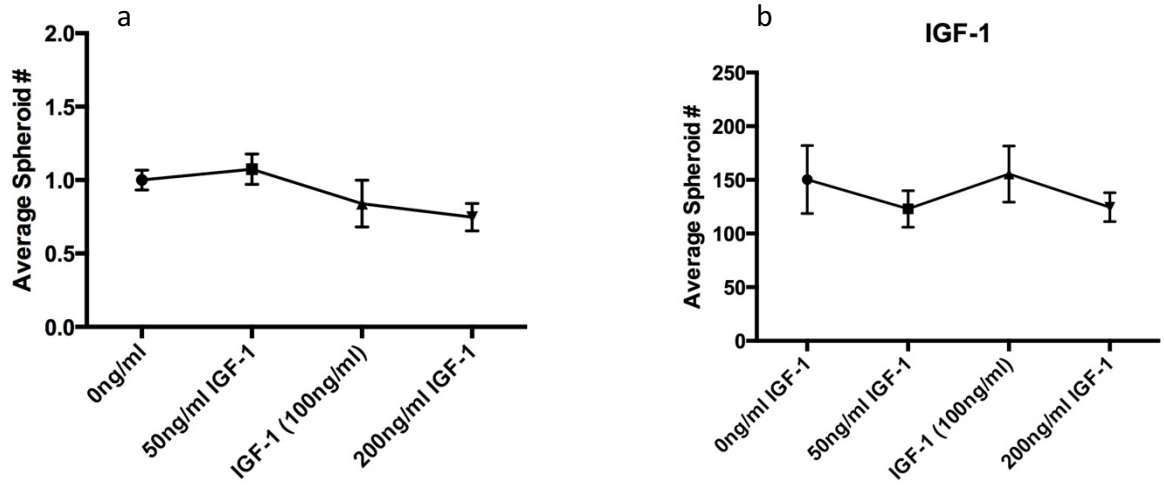

Figure 19. IGF-1 trials (Cell Line 1) a) Cumulative P0-P2 b) P0 only

IGF-1 has been shown to increase the number of Intestinal Stem Cells (ISC) in both a pre- and post-injury setting [6]. The range of concentrations used were based on a publication by Van Landeghem et. al (2015). No significant data was shown to improve survival and growth across all concentrations.

Dexamethasone

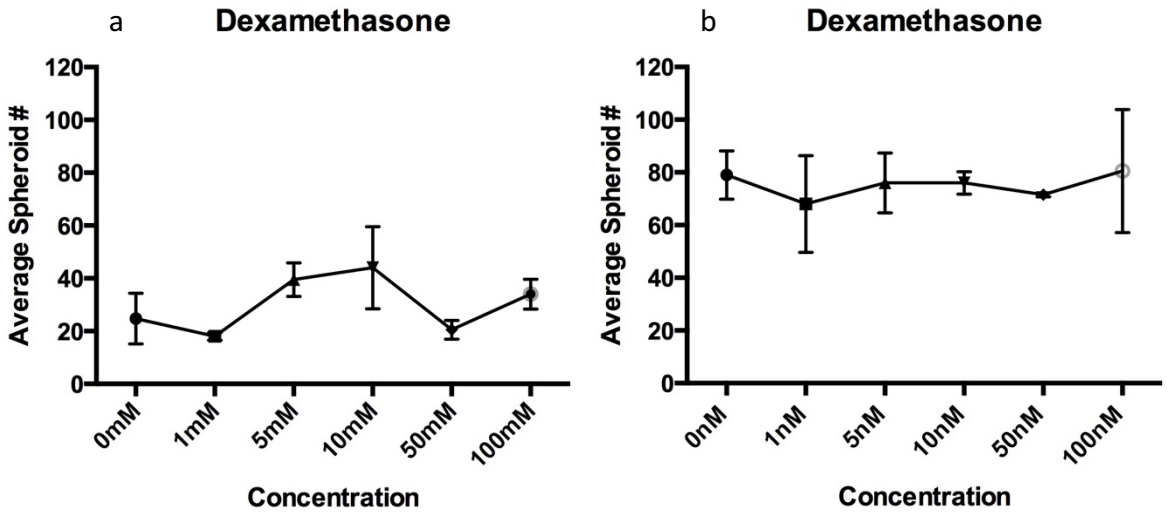

Figure 20. P0 Trials a) Trial 1 b) Trial 2

In an effort to discover and incorporate drugs that can be used in future in-vivo applications, an FDA-approved drug called Dexamethasone was tested. Determining the range of concentrations proved to be a challenging task, due to the lack of prior literature for this application. Therefore, a very broad range of values were tested. The results from trial 1 were not deemed significant, so in order to ensure threshold amounts had not been surpassed, concentrations were switched from mM to nM for trial 2. Despite the adjustment, dexamethasone did not substantially influence the growth of spheroids.

Insulin

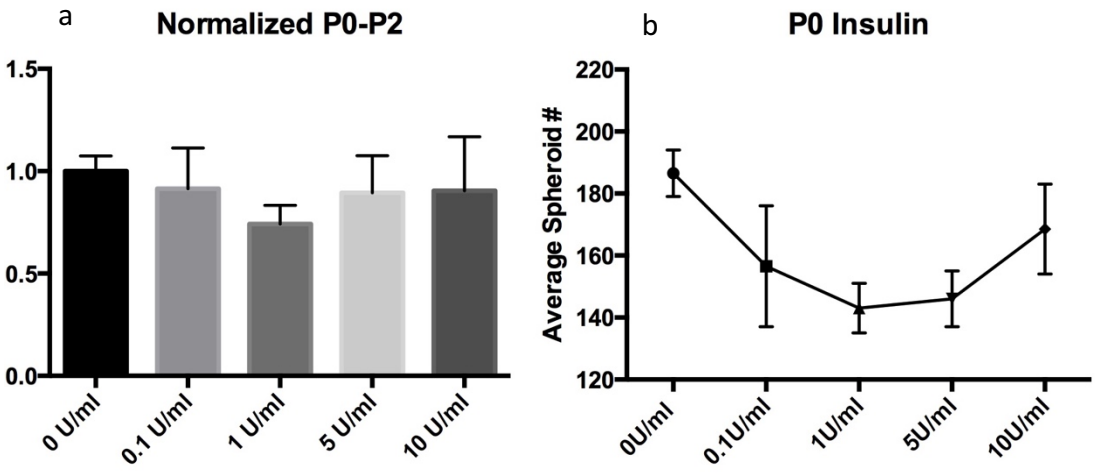

Figure 21. Insulin Trials a) Cumulative b) P0

Prior studies have shown a link between the activation of the Wnt signaling pathway and insulin sensitivity [10]. Given that Wnt activation has been shown to increase LGR5+ populations in crypt to spheroid conversions [9], the application of insulin to cell culture media was tested and observed. In this case, the concentrations once more, spanned a larger range of values due to lack of prior data available for reference. Interestingly, the graph displayed a downward parabolic trend across varying concentrations. Overall, insulin did not have a positive effect on growth.

BAC

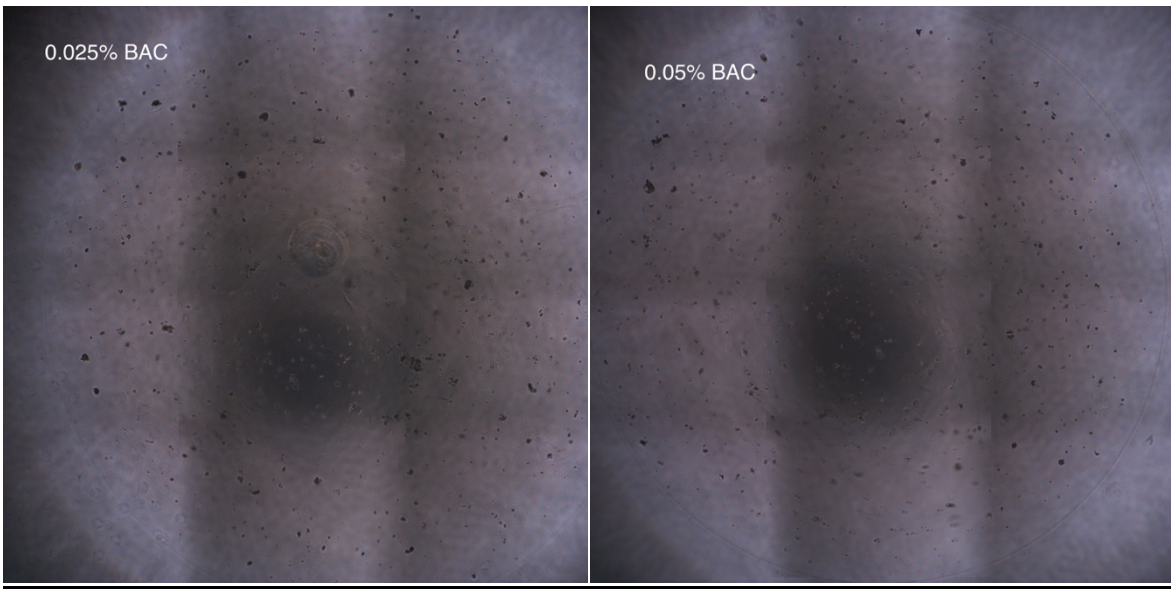

Figure 22 Images of the spheroid particles post-BAC exposure

Benzalkonium Chloride (BAC) is another compound tested. Due to the total lack of growth with such small amounts, it was not tested any further. The result was not surprising, due to BAC being used for ablating cell surfaces. It was beneficial in the sense that one is able to gauge the sensitivity of the spheroids to such small amounts.

OACD

From the screening portion of the experiment, it became apparent that EGF, Noggin, R-Spondin, and Y-27632 were the only necessary factors to be incorporated into the design of the OACD. Since E, N, R, Y were the only factors to be optimized, an OACD based on a 4 factor, resolution IV design was constructed. The OACD used is composed of a 2-level fractional factorial and a 3-level orthogonal array design.

4	2_{IV}^{4-1}	8	$D = ABC$	OA(9)	(1-4)

Run	a	b	c	d
1	−1	−1	−1	−1
2	−1	−1	1	1
3	−1	1	−1	1
4	−1	1	1	−1
5	1	−1	−1	1
6	1	−1	1	−1
7	1	1	−1	−1
8	1	1	1	1

OA(9)

Run	a	b	c	d
9	−1	−1	−1	−1
10	−1	0	0	1
11	−1	1	1	0
12	0	−1	0	0
13	0	0	1	−1
14	0	1	−1	1
15	1	−1	1	1
16	1	0	−1	0
17	1	1	0	−1
18	0	0	0	0
19	0	0	0	0

Figure 23. OACD constructed for spheroid growth optimization. (Courtesy of Dong-Keun Lee & Theodore Kee)

The concentrations or levels in the OACD correspond to the numerical values as follows: -1 is the minimum concentration, 0 is the concentration between the min. & maximum, and 1 is the maximum concentration. The OACD incorporated a duplicate run for the negative control and the mid-point (run #9 and run #19). However, since each condition or run is carried out in duplicate wells, it was not necessary. The negative control used for each trial was 0xENRY (i.e. no growth factor added).

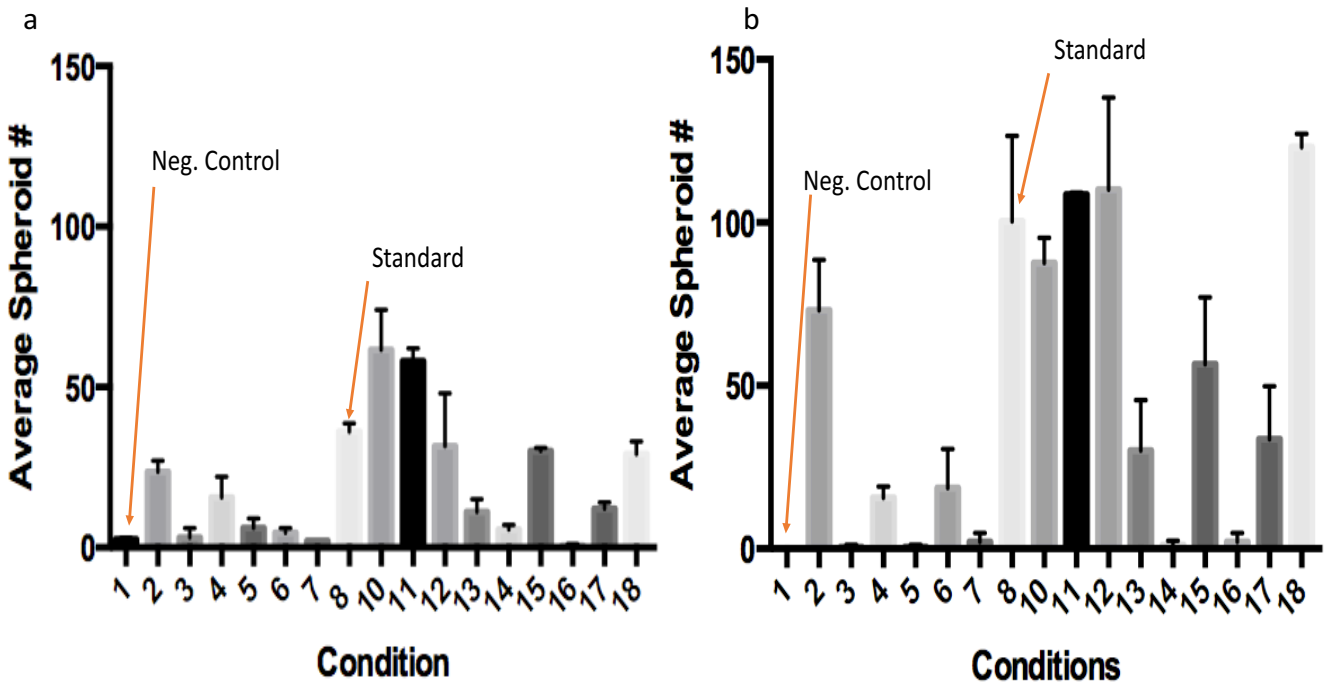

1	2	3	4	5	6	7	8	10	11	12	13	14	15	16	17	18
2	20	0	9	3	3	2	31	74	54	48	7	7	29	0	14	33
3	27	6	22	9	6	2	33	49	62	15	15	4	31	1	10	25
							43									
							37									

1	2	3	4	5	6	7	8	10	11	12	13	14	15	16	17	18
0	62	1	18	1	27	4	79	82	109	130	19	0	71	0	22	126
0	84	0	13	0	10	0	122	93	108	90	41	2	42	4	45	120
							124									
							76									

Figure 24. P0 Results of the OACD trials a) Trial 1 b) Trial 2

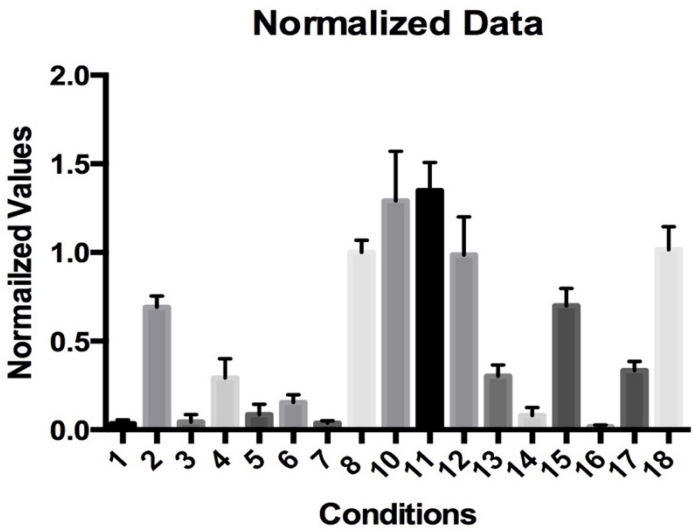

Figure 25. Cumulative results of the Cell Line 1 OACD trials. (Note: Both trials were conducted on Cell Line 1, which was the original cell Line)

Multiple trials were performed at P0 based on the OACD in order to verify the results were indeed reproducible at both lower and higher spheroid numbers. Data from both trials was normalized according to the standard concentration (run #8) and combined (Figure 25). Conditions 2, 10, 11, 12, 15, and 18 showed growth that was similar to the standard condition (condition 8). Since both R-Spondin and Noggin were the most expensive growth factors, conditions that used significantly less Noggin and R-Spondin (conditions 10, 12, &18) were further explored. Another trial was performed focusing on these three conditions, with slight modifications to each condition (denoted with the letter A next to the condition) and their ability to be passaged. Another cell line was also tested in tandem in order to observe the reproducibility of the results given the sample variation.

Condition	E	N	R	Y
10	0x	0.5x	0.5x	1x
10A	0x	0.25x	0.35x	1x
12	0.5x	0x	0.5x	0.5x
12A	0.5x	0.25x	0.5x	0.5x
18	0.5x	0.5x	0.5x	0.5x
18A	0.5x	0.25x	0.25x	0.5x

Table 1. E,N,R,&Y concentrations for each condition in the post-OACD exploratory trial

Although this modification step is not necessary for the data to be fit to the second order equation, it is beneficial to observe cell response while simultaneously altering multiple components. Given that Noggin and R-Spondin contribute to a large portion of cost, these factors were the primary interest in designing the modified conditions. Both conditions 10A and 18A

were designed in order to observe the growth potential with a reduction in Noggin in conjunction with a reduction in R-Spondin. Condition 12A was designed in order to verify the difference in post-passaging survival when comparing 0x Noggin and 0.25x Noggin.

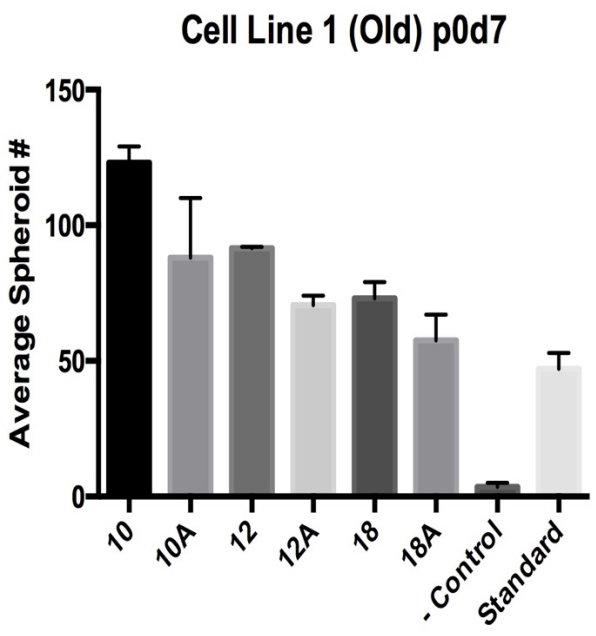

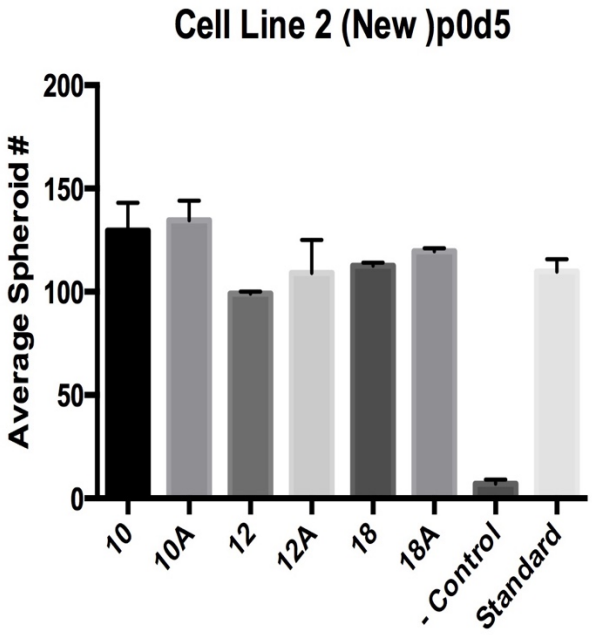

10	10A	12	12A	18	18A	- Control	Standard
117	66	92	67	79	67	2	59
129	110	91	74	67	48	5	31
							46
							52

10	10A	12	12A	18	18A	- Control	Standard
143	144	98	93	111	118	5	106
116	125	100	125	114	121	9	126
							110
							97

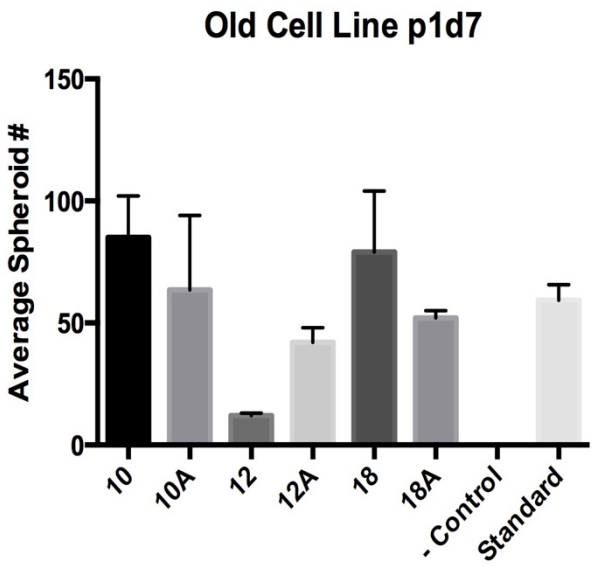

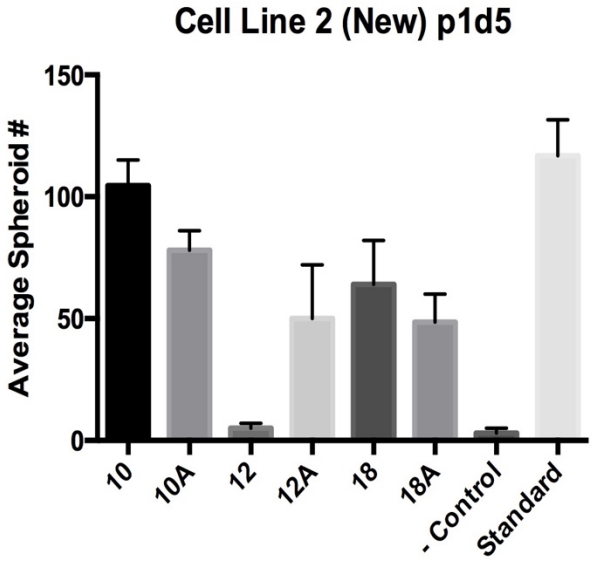

10	10A	12	12A	18	18A	- Control	Standard
68	94	13	48	104	49	0	78
102	33	11	36	54	55	0	57
							52
							50

10	10A	12	12A	18	18A	- Control	Standard
115	86	3	72	82	60	5	139
94	70	7	28	46	37	1	145
							98
							85

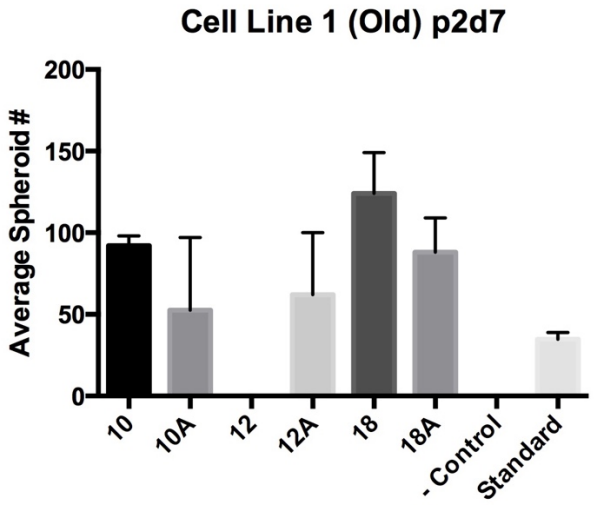

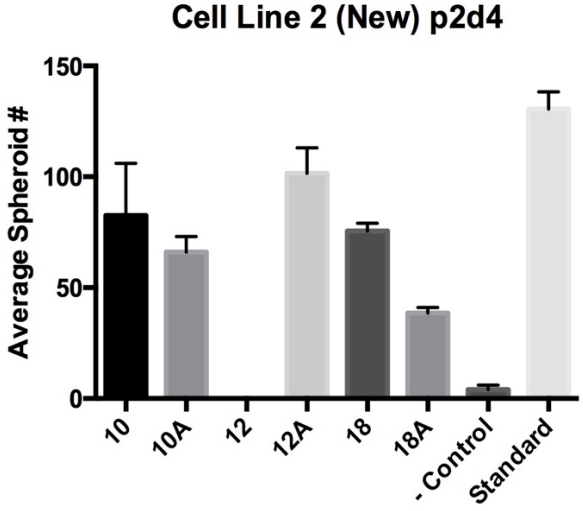

10	10A	12	12A	18	18A	- Control	Standard
98	97	N/A	100	149	109	0	28
86	8	N/A	24	99	67	0	44
							39
							27

10	10A	12	12A	18	18A	- Control	Standard
106	59	N/A	90	72	41	6	147
59	73	N/A	113	79	36	2	129
							110
							136

Figure 26. Graphical representations of post-OACD exploratory trials. 2 cell lines were tested from P0-P2.

At P0, both cell lines exhibited differences in numbers and trends. In wells with the original cell line labeled "Cell Line 1 (old)", at P0 all the modified conditions seemed to be less confluent than that of the unmodified conditions. The opposite was observed in wells labeled "Cell Line 2 (New)". After the initial passage, the cells in condition 12 with 0x noggin experienced poor growth across both cell lines- to the point that they could not be passaged any further. The cells in condition 12A with 0.25x however, displayed greater growth and survived passaging to P2. Different conditions were favored by different cell lines. For example, in Cell Line 1 condition 18 did the best in both P1 & P2, while in Cell Line 2 none of the conditions did better than the standard. It is important to note that the response profile from the cumulative P0-P2 modified condition data was not used to create the equation modeling spheroid growth. Interestingly, well to well variation played a larger role during this round of experimentation. The source for this error would be the particle seeding density during passaging. Each condition contains a total of ~ 600 particles (~300 particles/well x 2), so if one well contains more than 300 particles, then the other well contains less than 300 particles (both wells are plated from the same Eppendorf tube). The wells with more particles, will give more spheroids and of course the opposite is true. So long as the total is 600 particles for both wells combined, then the average value can be taken.

The response profile from the P0 OACD using the original cell line was used to obtain the coefficients of the 2nd order equation:

$$Spheroid\# = 1.6501 + 333.74E - 52.1N + 52.906R + 0.57285Y - 100.25EN$$
$$- 23.417ER - 107.75EY + 122.42NR + 41.086NY + 173.92RY$$
$$- 210.7E^2 + 25.506N^2 - 139.04R^2 - 20.369Y^2$$

The coefficients for each term in the equation show the growth factor interactions in the system, and whether or not it supports spheroid growth, or inhibits it. Each first-order term shows the interaction of a single growth factor molecule with each spheroid. The second-order terms display the interaction of multiple molecules of a single growth factor on a single spheroid. The cross-interaction terms show the spheroidal interaction with multiple molecules from different growth factors. The statistical information for each term obtained is outlined in Table 2 (below).

	Estimate	SE	tStat	p-Value
(Intercept)	1.6501	10.942	0.1508	0.88157
E	333.74	96.751	3.4495	0.0024018
N	-52.1	37.169	-1.4017	0.17562
R	52.906	96.751	0.54683	0.59026
Y	0.57285	96.751	0.0059209	0.99533
E:N	-100.25	40.519	-2.4741	0.021972
E:R	-23.417	42.587	-0.54986	0.58822
E:Y	-107.75	42.587	-2.5301	0.019466
N:R	122.42	40.519	3.0213	0.0064977
N:Y	41.086	40.519	1.014	0.32213
R:Y	173.92	42.587	4.0838	0.00053177
E^2	-210.7	60.921	-3.4586	0.0023507
N^2	25.506	29.537	0.86352	0.39761
R^2	-139.04	60.921	-2.2822	0.033006
Y^2	-20.369	60.921	-0.33436	0.74143

Table 2. Statistical Data from the linear regression analysis

The p-value for each term was analyzed and the p-values were elevated for some of the terms were high. Therefore, a stepwise regression was performed where the second order and cross-interaction terms with large p-values were removed. The predicted number of spheroids from the stepwise regression were compared with the values obtained from the linear regression. The resulting output values from both the stepwise regression and the linear regression were similar (see Supplemental Materials), showing that the terms removed (ER, NY, N^2, Y^2) did not significantly contribute to the model.

Condition	E	N	R	Y
10	0x	0.5x	0.5x	1x
12	0.5x	0x	0.5x	0.5x
12A	0.5x	0.25x	0.5x	0.5x
18	0.5x	0.5x	0.5x	0.5x
RP2	0.3x	1x	1x	1x
RP1000	0.4x	0.9x	0.5x	0.9x
RP2000	0.4x	0.6x	1x	0.5x
RP3000	0.5	0.1	0.3	0.4
RP4000	0.5	0.4	0.3	0.2

Table 3. OACD and regression prediction conditions and their concentrations.

From the predicted values, new conditions were added. A total 5 new conditions (RP2, RP1000, RP2000, RP3000, & RP4000) were used with a varying range of concentrations for each component (see 'regression predictions' in Supplemental Materials). The most promising conditions from the OACD (condition 10 & 18) were also tested side by side with these newer

conditions. Condition 12 & 12 A were compared once more for the sake. (Note: the standard condition was predicted to have 94.84 spheroids)

Condition	Predicted # of Spheroids
RP2	231.6153302
RP1000	134.708451
RP2000	116.9383746
RP3000	107.4929774
RP4000	100.1972546

Table 4. Predicted spheroid numbers given by the derived polynomial

In order to account for the noise factors, certain steps were taken in this final experiment. In order to account for the well to well variation, the output was measured in terms of % spheroids formed in each condition (# of spheroids/600 x 100), as opposed to the average # of spheroids. Multiple trials were conducted on each cell line in order to observe and account for trial variation. In order to once more view the effects of sample variation, an even newer cell line (Cell Line 3) replaced Cell Line 2.

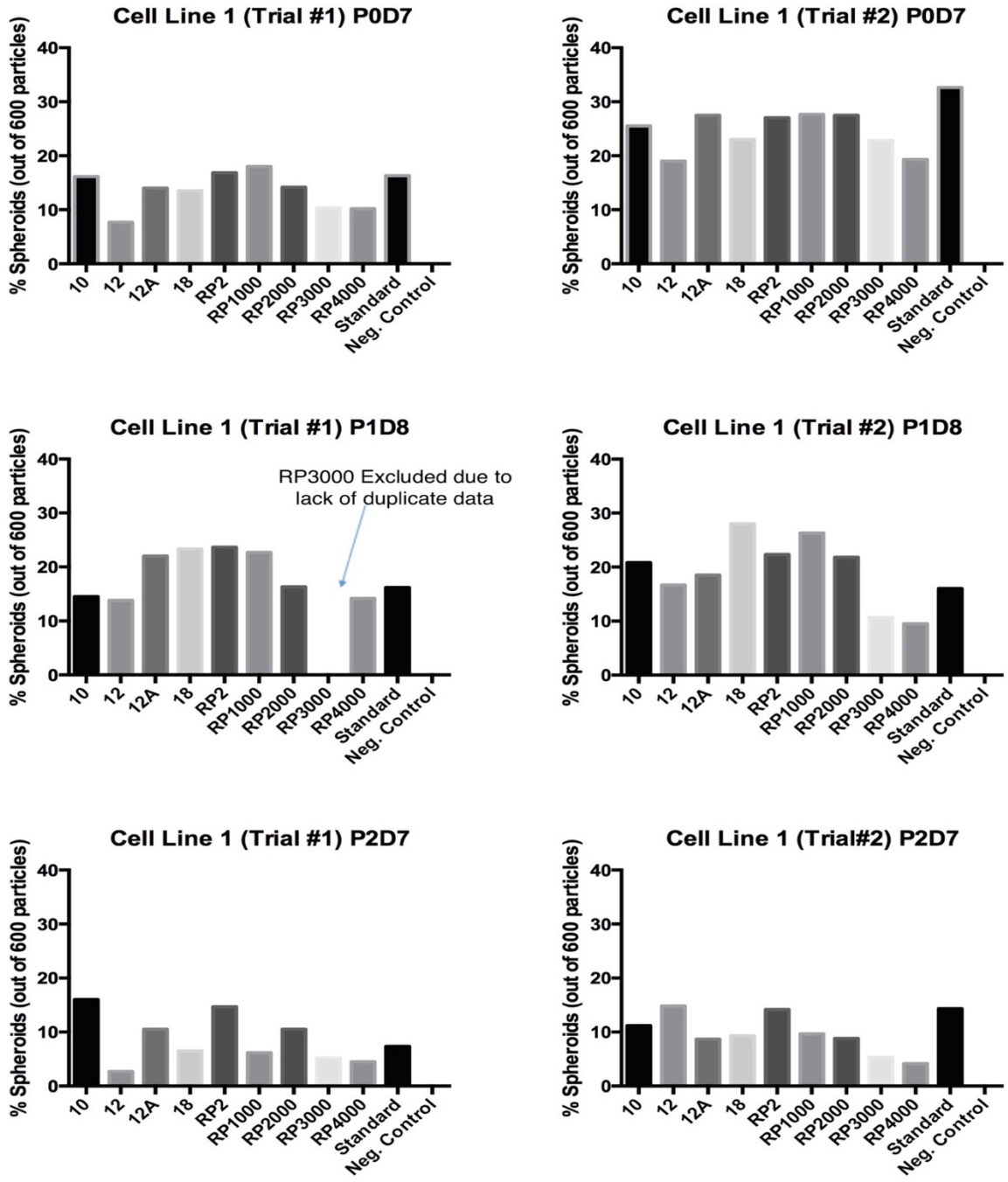

Figure 27. Cell Line 1 Final Trials

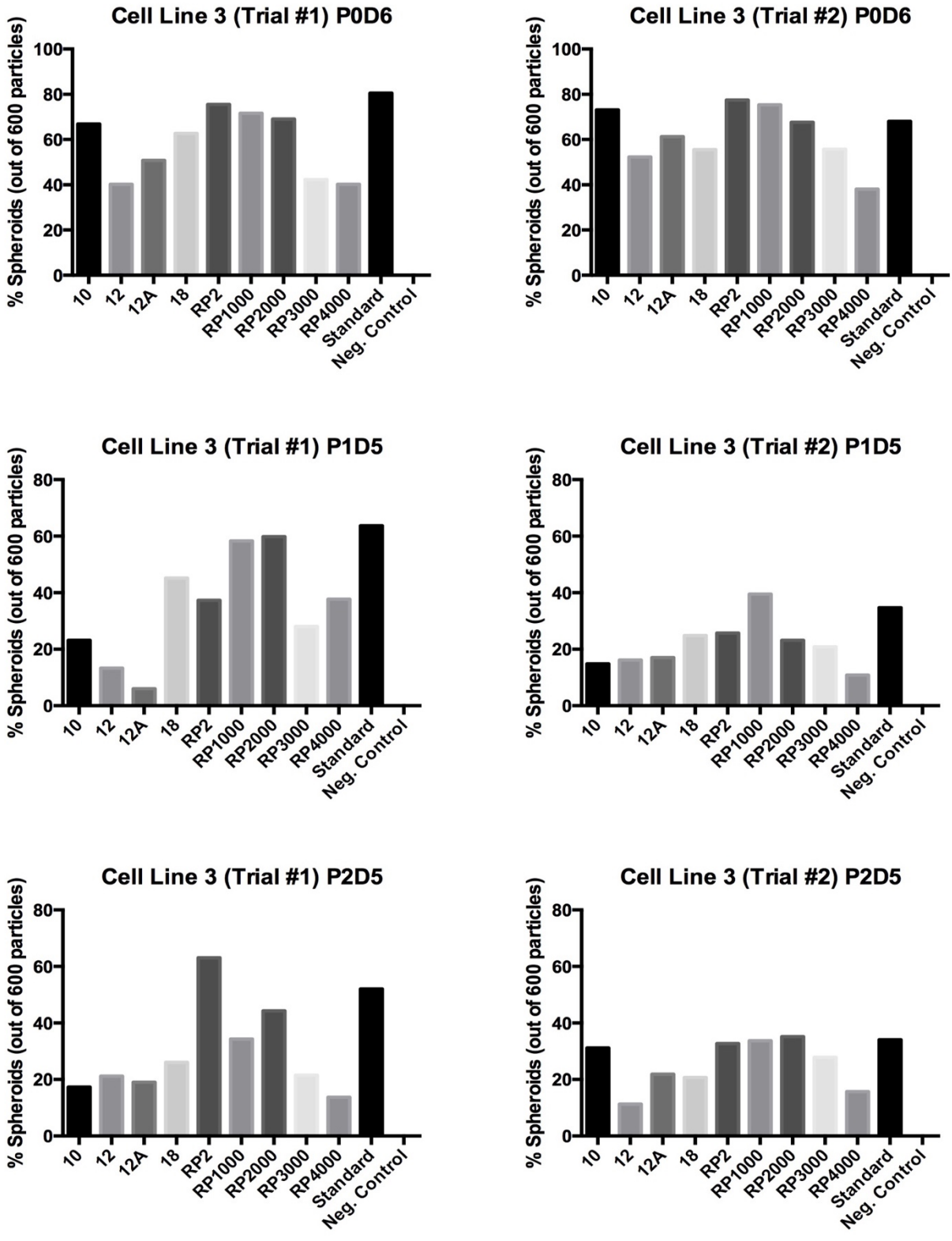

Figure 28. Cell Line 3 Final Trials

At p0, across both cell lines, the results are relatively consistent. As seen in the graphed results for Cell Line 1 and Cell Line 3 (Figure 27 & 28) the equation accurately predicts the order of optimal conditions by exhibiting a direct correlation between the RP condition and spheroid numbers. In other words, as conditions vary from RP2 to RP4000, spheroid levels decrease. It is worth noting however, that the patterns between the cell lines and even the trials, diminishes at P1 and P2. This reveals the crucial role that cell passaging plays in optimization. Nevertheless, P0 data is most relevant to this experiment because of the fact that the equation was constructed using P0 OACD data. The conditions that typically showed growth at level similar to the standard at P0, include: RP2, RP1000, and condition 10. To further verify the results in a more quantitative manner, RNA was extracted at P0, and the RNA levels were quantified using a Nanodrop 2000c (Figure 29).

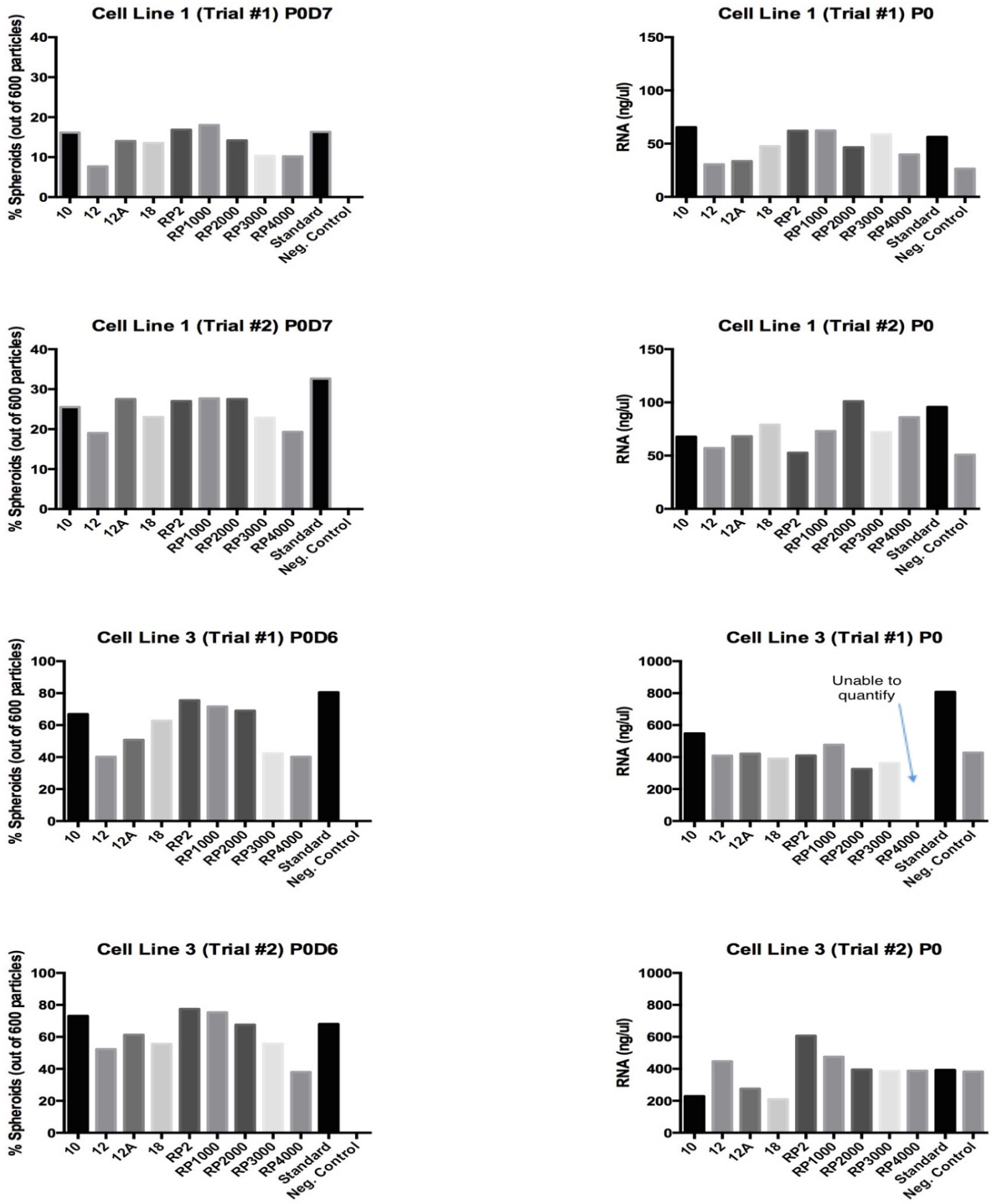

Figure 29. Comparison of P0 RNA vs. ImageJ analysis methods (Cell LIne 1 & Cell Line 3)

The comparison between the imageJ cell counting and the RNA quantification data revealed a

correlation in patterns between the two methods, yet many differences were also observed. The fact that the imageJ analysis uses data from both wells (before passaging and RNA extraction) in each condition, while RNA is quantified from only one well (the other well is passaged), can account for some of the differences. The negative control was also elevated, which indicates a potential limit in the accuracy of the Nanodrop. In order to verify that the RNA value for the negative control was not as elevated as indicated, a RNA quality control check was performed at the UCLA Clinical Microarray Core Facility for the negative control and standard condition of one sample (Cell Line 3, Trial #1).

CMC

Standard (conc. ng/ml)	**-Control**(conc. ng/ml)
393 ng/ul	5.46 ng/ul
Standard (RINe)	**- Control (RINe)**
9	Out of Range

Table 5. Cell Line 3 Standard & Negative control RNA QC

Nanodrop

Standard (conc. ng/ml)	**- Control** (conc. ng/ml)
807.5 ng/ul	428 ng/ul

Table 6. Cell Line 3 Standard & - control Nanodrop

The RNA QC proved that the concentration of the negative control was not as high as indicated in the Nanodrop quantification, but it also proved that the reading for the standard was not accurate either. The RNA Integrity Number equivalent (RINe) also proved that the RNA concentration reading from the negative control was not significant due to it being too low/out of the reading range.

Conclusion

The goal of this experiment was to utilize an efficient, reproducible, and user-friendly platform in order to optimize intestinal stem cell growth conditions. This goal was accomplished using the 2nd order equation constructed from data produced by a response profile from an OACD. Three conditions that seemed to perform the best were RP2, RP1000, and 10. However, the performance of these conditions varied from trial to trial and sample to sample. Also, the number of spheroids predicted by the linear regression were not accurate. Nevertheless, data was acquired in support of the idea of using lower concentrations of growth factors to promote growth at an efficiency similar to the standard/conventional concentrations already used. A few of the conditions substantially cut cost, thus preserving precious resources (Table 7).

Condition	Cost
Standard	$6.085/ml
RP2	$6.057/ml
RP1000	$3.457/ml
10 (From OACD)	$3.058/ml

Table 7. Estimated cost of each condition

RP2 reduces EGF concentration by 70%, however, it only reduces cost by only 0.46% ($0.03/ml). This is due to EGF only costing an estimated $0.04/ml. RP1000 reduces cost by an estimated 43.2%, which translates to $2.63/ml. Condition 10 reduces cost by 49.7%. The reduction in R-Spondin ($5/ml) is responsible for the massive price difference between the

standard and conditions: 10 and RP1000. It is important to note the need to optimize conditions for each sample separately and each cell passage, due to the variability in response.

Future Work/Improvements

Although the desired function of the equation was achieved, potential improvements to this project can be implemented for greater results.

The first improvement would be to optimize conditions for each passage, and increase the number of passages. The role of passaging became clear as the project progressed. Variability in outcomes was observed after only two passages- in some cases only one passage affected data output. Given that the project was only limited to two passages, it restricted the ability to observe long-term effects of growth factor concentration modifications. Nonetheless, it is important to recognize both the monetary and time cost of increasing the number of passages in the experiment, given the large number of conditions.

Another improvement to the work would incorporate a larger number of samples. Using a larger number of samples would allow for greater availability of cell lines to optimize and conduct experiments on, and aid in accounting for different responses due to sample variability.

REFERENCES

1. Rescigno, M. (2015). Intestinal epithelial spheroids: new tools for studying gastrointestinal diseases. *Gut*, *64*(6), 859-860.

2. Barker, N. (2014). Adult intestinal stem cells: critical drivers of epithelial homeostasis and regeneration. *Nature reviews Molecular cell biology*, *15*(1), 19-33.

3. Barker, N., van Es, J. H., Kuipers, J., Kujala, P., van den Born, M., Cozijnsen, M., ... & Clevers, H. (2007). Identification of stem cells in small intestine and colon by marker gene Lgr5. *Nature*, *449*(7165), 1003-1007.

4. Sato, T., Vries, R. G., Snippert, H. J., van de Wetering, M., Barker, N., Stange, D. E., ... & Clevers, H. (2009). Single Lgr5 stem cells build crypt villus structures in vitro without a mesenchymal niche. *Nature*, *459*(7244), 262-265.

5. Sato, T., van Es, J. H., Snippert, H. J., Stange, D. E., Vries, R. G., van den Born, M., ... & Clevers, H. (2011). Paneth cells constitute the niche for Lgr5 stem cells in intestinal crypts. *Nature*, *469*(7330), 415-418.

6. Van Landeghem, L., Santoro, M. A., Mah, A. T., Krebs, A. E., Dehmer, J. J., McNaughton, K. K., ... & Lund, P. K. (2015). IGF1 stimulates crypt expansion via differential activation of 2 intestinal stem cell populations. *The FASEB Journal*, *29*(7), 2828-2842.

7. Elliott, E. N., & Kaestner, K. H. (2015). Epigenetic regulation of the intestinal epithelium. *Cellular and Molecular Life Sciences*, 72, 21, 4139-4156

8. Porter, E. M., Bevins, C. L., Ghosh, D., & Ganz, T. (2002). The multifaceted Paneth cell. *Cellular and molecular life sciences CMLS*, *59*(1), 156-170.

9. Yin, Xiaolei, et al. Niche-independent high-purity cultures of Lgr5+ intestinal stem cells and their progeny. *Nature methods* 11.1 (2014): 106-112.

10. Abiola M, Favier M, Christodoulou-Vafeiadou E, Pichard A-L, Martelly I, et al. (2009) Activation of Wnt/b-Catenin Signaling Increases Insulin Sensitivity through a Reciprocal Regulation of Wnt10b and SREBP-1c in Skeletal Muscle Cells. *PLoS ONE* 4(12): e8509. doi:10.1371/journal.pone.0008509

11. Xu, H., Jaynes, J., & Ding, X. (2014). Combining two-level and three-level orthogonal arrays for factor screening and response surface exploration. *Statistica Sinica*, *24*, 269-289.

12. Zarrinpar, A., Datta, N., Eriksen, C., Weigle, K., Agopian, V., Kaldas, F., Farmer, D., ... Ho, D. (2016). Individualizing liver transplant immunosuppression using a phenotypic personalized medicine platform. *Science Translational Medicine*, 8, 333.

13. Hann Wang, Dong-Keun Lee, Kai-Yu Chen, Jing-Yao Chen, Kangyi Zhang, Aleidy Silva, Chih-Ming Ho, Dean Ho (2015). Mechanism-independent optimization of combinatorial nanodiamond and unmodified drug delivery using a phenotypically driven platform technology.*ACS Nano*, 9(3), 3332–3344.

14. Jaynes, J., Ding, X., Xu, H., Wong, W. K., & Ho, C. M. (2013). Application of fractional factorial designs to study drug combinations. *Statistics in medicine*, *32*(2), 307-318.

(Linear Regression, Stepwise Regression, and Regression Prediction Excel files in

"Supplementary Materials" provided by Theodore Kee and Michael Dinh)